Highly active and stable AuNi dendrites as an electrocatalyst for the oxygen reduction reaction in alkaline media

Wang, Jiali; Chen, Fuyi; Jin, Yachao; Johnston, Roy L.

DOI:
10.1039/c6ta07519c

Document Version
Peer reviewed version

Citation for published version (Harvard):
Wang, J, Chen, F, Jin, Y & Johnston, RL 2016, 'Highly active and stable AuNi dendrites as an electrocatalyst for the oxygen reduction reaction in alkaline media', *Journal of Materials Chemistry A*, vol. 4, no. 45, pp. 17828-17837. https://doi.org/10.1039/c6ta07519c

Journal of Materials Chemistry A

Accepted Manuscript

This article can be cited before page numbers have been issued, to do this please use: J. Wang, F. Chen, Y. Jin and R. L. Johnston, *J. Mater. Chem. A*, 2016, DOI: 10.1039/C6TA07519C.

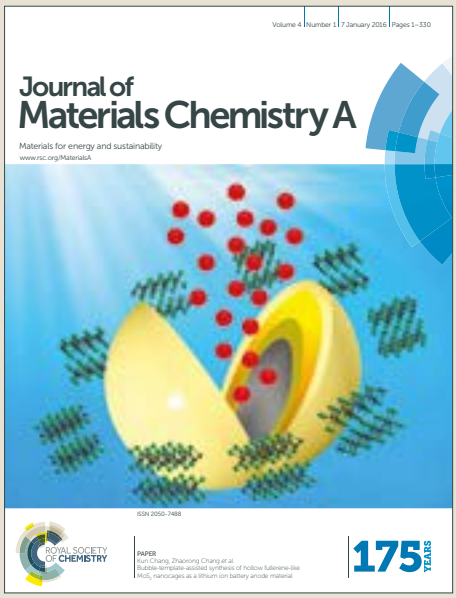

ROYAL SOCIETY OF CHEMISTRY

rsc.li/materials-a

View Article Online
DOI: 10.1039/C6TA07519C

Journal Name

ARTICLE

Highly Active and Stable AuNi Dendrite as Electrocatalyst for Oxygen Reduction Reaction in Alkaline Media†

Received 00th January 20xx,
Accepted 00th January 20xx

DOI: 10.1039/x0xx00000x

www.rsc.org/

Jiali Wang,[a] Fuyi Chen,*[a] Yachao Jin,[a] and Roy L. Johnston[b]

Bimetallic AuNi nanodendrite catalysts have been prepared for oxygen reduction reaction (ORR) in alkaline media by the facile electrodeposition and electrochemical dealloying method. The dealloyed AuNi catalyst consists of hierarchical dendrites with high electrochemical active surface area. The half-wave potential ($E_{1/2}$) of the dealloyed AuNi catalyst is 0.896 V vs. RHE, exhibiting about 67 and 27 mV positive shift relative to the commercial Pt/C and as-prepared (before dealloying) AuNi catalysts, respectively. Compared to commercial Pt/C catalyst, the dealloyed AuNi achieves a 2.8-fold improvement in specific activity at 0.8 V vs. RHE and suffers less degradation of the ORR activity after 5,000 potential cycles. The ORR catalyzed by bimetallic AuNi catalyst proceeds through a four-electron pathway in basic solution. TEM and XPS characterizations indicate that the enhancement of ORR activity is attributed to the favorable morphology and electronic effect caused by the incorporation of Ni atoms into Au substrate. Dealloyed AuNi hierarchical dendrites possess the great application potential as cathode electrocatalysts in the metal-air batteries and alkaline fuel cells due to the facile preparation, high ORR activity and long-term cycling durability.

Introduction

Renewable energy technologies, such as metal-air batteries and alkaline fuel cells, have garnered considerable interests because they are expected to become the reliable sources of clean energy in both mobile applications and energy conversion/storage devices.[1-4] It is well acknowledged that the kinetics of oxygen reduction reaction (ORR, $O_2 + 2H_2O + 4e^- \rightarrow 4OH^-$) at the cathode of these electrochemical devices is intrinsically sluggish, thus, this reaction requires a large amount of catalysts to achieve adequate energy efficiency.[1-5] Hitherto, platinum (Pt) has been regarded as the state-of-the-art catalyst applied in such technologies. However, Pt and Pt-based alloys suffer from severe durability problems,[3, 6] together with high cost and scarcity,[7, 8] limiting their wide-spread application in industry. Therefore, enormous efforts have been dedicated to develop the non-platinum catalysts with more economical metals and higher catalytic activity.[4, 6, 9-12]

Among various non-platinum cathode catalysts, gold (Au) has attracted substantial attention.[13-17] Numerous studies demonstrate that gold (Au) at the nanoscale exhibits good catalytic activity than the bulk Au for ORR.[15] Tang et al. presented a novel strategy to grow ultrafine Au clusters (less than 2 nm) on the reduced graphene oxide (rGO) sheets, exhibiting excellent electrocatalytic activity toward ORR.[13] Au/rGO hybrid consisting of Au nanodendrites (~30 nm) was successfully synthesized in Chen's group, which had a comparable onset potential to commercial Pt/C catalyst and showed a dominant four-electron pathway for ORR.[14] However, these nanosized Au catalysts with high surface energy are tend to dissolve, aggregate and sinter during catalysis,[13] moreover, Au nanoparticles used alone hardly have comparable or better ORR catalytic activity than that of commercial Pt/C catalyst.[13, 14] Previous literatures reported that the ORR activities of metal catalysts were related to the oxygen adsorption energies, and both higher and lower oxygen adsorption energies had negative effects on the ORR activity.[18, 19] According to the volcano plot reported by Nørskov,[18] there is still significant scope to improve the catalytic activities of metal catalysts through changing their oxygen adsorption energies, which is also manifested in the shift of d-band center with respect to the Fermi level.[19] Downshift of the d-band center location with respect to Fermi level indicates that the oxygen absorption energy is lowered, and the vice versa for the unshift of d-band center. For example, Pt is recognized as the state-of-the-art catalyst with slightly strong oxygen binding energy, it has been approved that the ORR activity of Pt could be substantially improved by forming the Pt-M (M= Fe, Co, or Ni) alloys due to the downshift of d-band center as a result of the surface compressed strain and/or electronic effects.[20, 21] Based on the volcano plot, it is widely accepted that the poor activities of Au and Ag towards ORR are attributed to the particularly weak binding energies of oxygen. Recent researches have showed that the oxygen adsorption energy of Ag can be improved through doping the transition metals (*i.e.*, Cu) into Ag due to the upshift of d-band center with respect to Fermi level, and the

[a] State Key Laboratory of Solidification Processing, Northwestern Polytechnical University, Xian, 710072, China. E-mail: fuyichen@nwpu.edu.cn; Tel./fax: +86029-88492052
[b] Department of Chemistry, University of Birmingham, Birmingham, B15 2TT, UK. E-mail: r.l.johnston@bham.ac.uk.

† Electronic supplementary information (ESI) available: parameters optimization, ORR polarization curves, SEM images and EDX results of Au_xNi_y, reproducible ORR curves, ORR polarization curves, K-L plots and electron transfer numbers of commercial Pt/C and Pure Au, RDE electrochemical measurements and Koutecky-Levich plots of all Au_xNi_y catalysts, TEM images before and after cycling, and comparison of ORR activities. See DOI: 10.1039/x0xx00000x

View Article Online
DOI: 10.1039/C6TA07519C

resulted AgCu alloy showed enhanced ORR activity compared to the monometallic Ag.[22-24] Thus, it is reasonable to predict that alloying Au with transition metals (Ni, Co, Fe, etc.) with well-controlled sizes, components and geometrical structures could be one of the viable avenues to dramatically improve oxygen adsorption energy of Au to enhance the ORR activities.

As one of the 3d metals, nickel (Ni) has been widely used to improve the catalytic activities of Pt,[25-27] Pd[6, 28, 29] and Ag,[30] etc.. AuNi alloys have also been studied by researchers in the field of catalysis.[31-35] Hosseini et al. designed the nanostructured Cu/Ni/AuNi catalyst using the electrodeposition process followed by galvanic replacement technique. The electrocatalytic activity of Cu/Ni/AuNi electrodes for borohydride electrooxidation was much higher than that of flat Au catalyst.[32] Zeng et al. prepared well dispersive AuNi nanoparticles on graphite composite film, the nanoparticles exhibited the features of alloy and showed high electrocatalysis to hydroquinone.[33] Yang et al. reported that nanospheric particles of AuNi bimetal by a facile co-reduction and annealing synthesis route exhibited a greatly enhanced electrocatalytic activity toward oxygen reduction reaction than that of pure Au nanoparticles.[31] Naveen et al. fabricated AuNi@pTBA composite catalysts using the electrochemical deposition method and reported their better ORR catalytic activities and stabilities relative to the Pt/C catalyst.[35] Although great progress has been achieved in AuNi alloys field, the current applications of AuNi alloys are focused on catalytic oxidation of borohydride,[32] hydroquinone[33] or glucose,[34] the reports for electrocatalytic oxygen reduction reaction are rare, resulting in the lack of systematically studies on the catalytic mechanism of AuNi catalysts for ORR. Moreover, the composite or polymer in the catalysts may block the electron transfer and mass transport, which seriously hamper their catalytic activities, and the simple and pure metallic catalysts without the influence of composite or polymer usually give more physicochemical insights into the catalyst design. Therefore, employing an effective synthesis method to fabricate pure metallic AuNi catalysts and then investigating their intrinsic ORR activities and catalytic mechanisms have become an interesting topic.

It is widely accepted that the unique physicochemical properties of nanostructured alloys depend markedly on their sizes and morphologies.[36, 37] Nanodendrite with highly hierarchical structure is a new class of multifunctional catalytic nanomaterials due to their high surface area, porous structure, high degree of conductivity and catalytic activity.[4, 37] It has been documented that this kind of morphology could be manipulated via the surface engineering,[38] such as electrodeposition.[35] Herein, we adopted the electrochemical deposition and dealloying method to fabricate a series of pure metallic Au_xNi_y (x = 1, y = 1, 2, 3) dendrite catalysts directly on the bare glassy carbon electrode, and examined their ORR activities and long-term cycling durability. The typical synthetic process of pure metallic AuNi catalysts is presented in Scheme 1. By adjusting the experimental parameters (details in the Supporting Information), the Au_1Ni_2 catalysts deposited at -0.6 V vs. SCE before and after dealloying exhibit remarkably enhanced catalytic activity. Therefore, Au_1Ni_2 catalysts deposited at -0.6 V vs. SCE before and after dealloying (labelled as the as-prepared and dealloyed AuNi catalysts for simplicity, respectively, in the discussion section) were taken for further experiments. The electrochemical parameters for

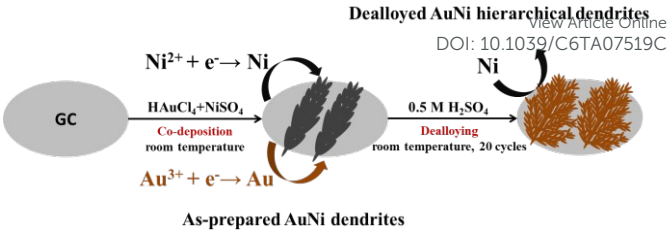

Scheme 1 Schematic illustration of the facile preparation of the AuNi hierarchical dendrites. The method is based on the electrodeposition of Au and Ni atoms in $HAuCl_4$ and $NiSO_4$ solution and the removement of surface Ni atoms through electrochemical dealloying process in H_2SO_4 solution. As-prepared AuNi electrode exhibits dendrites structure with less branches, while dealloyed AuNi electrode shows hierarchical dendrites, like "feather".

the preparation of pure metallic AuNi catalysts are drastically different from those observed in previous study with AuNi@pTBA composite catalysts,[35] presumably due to the absence of polymer. The electrochemical measurements demonstrate that the dealloyed AuNi catalyst outperforms the commercial Pt/C in both catalytic activity and durability. Because of the unique morphology advantage and the electronic effect, the dealloyed AuNi catalyst is further proved to be a promising electrocatalyst for the metal-air batteries and alkaline fuel cells.

Experimental section

Chemicals and materials

Gold(III) chloride trihydrate ($HAuCl_4$), nickel(II) sulfate hexahydrate ($NiSO_4{\cdot}6H_2O$), sodium sulfate (Na_2SO_4), sulfuric acid (H_2SO_4), and potassium hydroxide (KOH) were purchased from Tianjin Fuchen Chemical Reagent Co., Ltd. (China). Ethanol was purchased from Xi'an Shunda. All the chemicals used in this experiment were of analytical grade and used without any further purification. Pt/C catalyst (20 wt % Pt, fuel cell grade) was commercially available from Johnson Matthey Fuel Cells. All aqueous solutions were prepared with ultra-pure distilled water (18.25 MΩ cm). All experiments were carried out at room temperature.

Preparation of the AuNi catalysts

Prior to the preparation of the nanostructured AuNi dendrites, the glassy carbon electrode (GCE) was polished with 0.3 um alumina slurry and was sonicated for a few minutes in acetone and then in the distilled water. The GCE as the working electrode was placed facing a gold foil auxiliary electrode, and a saturated calomel electrode (SCE) was used as the reference electrode. The electrochemical depositions were performed in three different kinds of precursor solutions with 0.1 M Na_2SO_4 used as the support electrolyte. These precursor solutions contained 15 mM $HAuCl_4$ + 15 mM $NiSO_4$, 15 mM $HAuCl_4$ + 30 mM $NiSO_4$ and 15 mM $HAuCl_4$ + 45 mM $NiSO_4$, the corresponding samples were labelled as Au_1Ni_1, Au_1Ni_2 and Au_1Ni_3, respectively. The applied potentials during the electrodeposition were varied from -0.5 V to -0.7 V vs. SCE. The obtained products were taken out from the precursor solutions immediately after deposition process to prevent galvanic displacement reaction between Ni atoms and Au^{3+} cations and

washed carefully with distilled water, then dried by nitrogen at room temperature. After the potentiostatic deposition, the as-prepared samples were subject to the electrochemical dealloying process within the potential range of 0.0 to 1.6 V vs. Ag/AgCl in a N_2-purged 0.5 M H_2SO_4 solution at a scan rate of 50 mV s^{-1} for 20 cycles. Ag/AgCl electrode was used as the reference electrode during the dealloying process. For comparison purpose, pure Au was also deposited on the GCE under the same experimental conditions using the precursor solutions without $NiSO_4$. In order to ensure the reproducibility of each sample, we fabricated at least three separated samples for each kind of catalyst under the same experimental conditions. By calculating the transferred electron numbers during the deposition, the loading for the dealloyed AuNi catalyst was 0.17 mg.

Physical characterization

The phase and crystallinity of the AuNi dendrites were characterized using the X-ray diffraction (XRD) spectroscope with Cu Kα radiation (PANalytical X'Pert Pro MPD). The working potential and current employed were 40 KV and 40 mA, respectively. The morphologies and structures were observed by field emission scanning electron microscopy (SEM, FEI NovaSEM 450) and high-resolution transmission electron microscopy (HRTEM, FEI Tecnai F30). X-ray photoelectron spectroscopy (XPS) measurements were carried out on an ESCALAB 250 instrument (Al Kα, ultrahigh vacuum is 10^{-9}, hv = 1486.6 eV) to examine the surface components and electron structure, the binding energy was calibrated by the C 1s (284.5 eV).

Electrochemical characterization

Electrochemical measurements were carried out in 0.1 M KOH solutions at room temperature using the CHI 660C electrochemical workstation (Shanghai Chenhua Apparatus, China). The conventional three-electrode system including a glassy carbon electrode (d = 5 mm, geometric area 0.196 cm^2), Hg/HgO electrode and Pt wire electrode as the working, reference and counter electrode, respectively, was used. Linear scanning voltammetry (LSV) and cyclic voltammetry (CV) with a sweep rate of 10 mV s^{-1} from 0.2 to -0.8 V vs. Hg/HgO were conducted in O_2 and N_2-saturated 0.1 M KOH solutions. The rotation disk electrode (RDE) polarization curves in O_2-saturated 0.1 M KOH solution at different rotation rates were used to evaluate the number of electron transferred during ORR. The electrochemical active surface areas (ECSAs) of the Au-based catalysts were evaluated by integrating the charge associated with the reduction of a gold surface oxide monolayer in N_2-saturated 0.5 M H_2SO_4 solution in the range of 0.0 to 1.6 V vs. Ag/AgCl at a sweep rate of 50 mV s^{-1}, assuming the used charge density is 390 μC cm^{-2}.[39] The ECSA of commercial Pt/C catalyst was determined by measuring the charge associated with hydrogen adsorption/desorption in N_2-saturated 0.1 M KOH solution at a sweep rate of 50 mV s^{-1}, in which the charge density is 210 μC cm^{-2}.[37, 40] For the sake of clarity, all potentials in the paper were referred to the reversible hydrogen electrode (RHE) unless indicated.

Results and discussion

Fig. 1a shows the cyclic voltammetry (CV) curves of the dealloyed AuNi, as-prepared AuNi, pure Au and commercial Pt/C catalysts in 0.1 M KOH solution saturated with N_2 and O_2. For the dealloyed AuNi catalyst in the N_2-saturated solution, the CV curve is featureless over the potential range (other catalysts show the

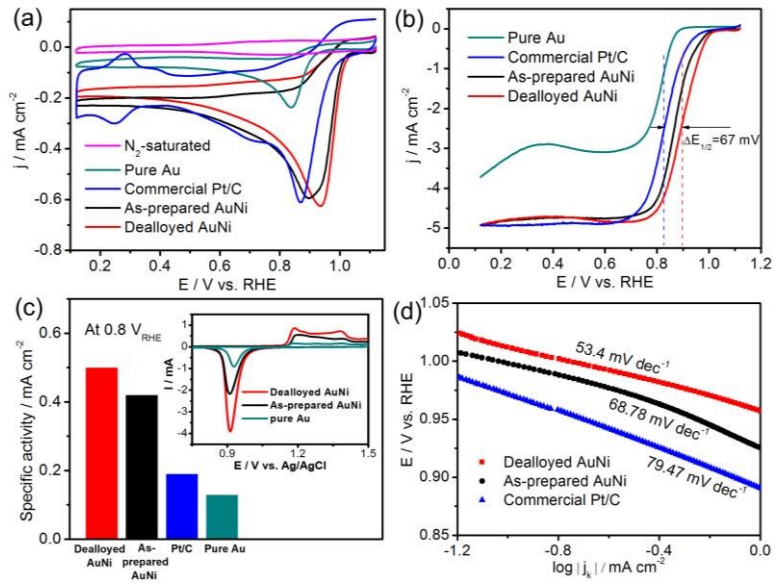

Fig. 1 Comparison of ORR activities of dealloyed AuNi, as-prepared AuNi, commercial Pt/C and pure Au catalysts at room temperature: (a) Cyclic voltammetry (CV) curves recorded in O_2-saturated 0.1 M KOH solution with a sweep rate of 10 mV s^{-1}, and CV of dealloyed AuNi in N_2-saturated 0.1 M KOH (magenta line). (b) ORR polarization curves recorded in O_2-saturated 0.1 M KOH solution with a sweep rate of 10 mV s^{-1} and a rotation rate of 1600 rpm. The current densities in both (a) and (b) were normalized in reference to the geometric area of the RDE (0.196 cm^2). (c) Specific activities at 0.8 V vs. RHE. The inset shows the CV curves of dealloyed AuNi, as-prepared AuNi and pure Au catalysts in N_2-saturated 0.5 M H_2SO_4 solution by sweeping the potential from 0.0 to 1.6 V vs. Ag/AgCl with a sweep rate of 50 mV s^{-1}. (d) Comparative mass-corrected Tafel plots of dealloyed AuNi, as-prepared AuNi and commercial Pt/C.

similar results, not shown). By contrast, when in the O_2-saturated solution, all catalysts exhibit apparent reduction current peak. A strong reduction current peak is found at 0.94 V for dealloyed AuNi catalyst, more positive than those of the as-prepared AuNi (0.9 V), commercial Pt/C (0.87 V) and pure Au catalysts (0.83 V), suggesting that the dealloyed AuNi catalyst exhibits higher catalytic activity toward oxygen reduction reaction. To further confirm the excellent ORR activity of the dealloyed AuNi catalyst, the linear sweep voltammetry (LSV) curves of these catalysts were measured at a rotating disk electrode (RDE) in O_2-saturated 0.1 M KOH solution with the rotation rate of 1600 rpm, as shown in Fig. 1b. As one of the most important descriptors in the quantitative assessments of ORR performance, the half-wave potential ($E_{1/2}$) of the dealloyed AuNi catalyst is 0.896 V, which has a 86, 67 and 27 mV positive shift compared to those of pure Au (0.810 V), commercial Pt/C (0.829 V) and as-prepared AuNi catalysts (0.869 V), respectively. In addition, the onset potential (E_{onset}) of the dealloyed AuNi catalyst is found to be the most positive among all the catalysts, which is close to those obtained from cyclic voltammetry measurements in Fig. 1a. The specific values for diffusion-limiting current density, $E_{1/2}$ and E_{onset} of these ORR catalysts are summarized and compared in Table. 1. These results highlight that oxygen reduction is markedly facilitated by the incorporation of non-noble metal Ni atoms into the Au substrate, and further improved by obtaining more active sites from the dealloying process.

As shown in the inset in Fig. 1c, the ECSA of dealloyed AuNi catalyst was measured to be 11.5 cm^2, which is about 1.3-fold higher than those of as-prepared AuNi and commercial Pt/C, respectively, and 3.4-fold higher than that of pure Au. The dealloyed AuNi catalyst displays a larger electrochemical active surface area and offers more accessible Au active sites in oxygen reduction, which mainly originates from the hierarchical dendrite-like nanostructure with higher level of porosity. We then calculated the specific activities (SAs) of these catalysts by normalizing kinetic current (I_k) to the ECSA at 0.8 V (Fig. 1c and Table 1). The values of the specific activities increase in the sequence: pure Au < commercial Pt/C < as-prepared AuNi < dealloyed AuNi. The dealloyed AuNi catalyst exhibits more than 2.8-fold enhancement in SA as compared to that of the commercial Pt/C catalyst at 0.8 V. Moreover, the kinetics of ORR can be further examined through the mass transport corrected Tafel plots. Fig. 1d gives the comparative Tafel plots of as-prepared AuNi, dealloyed AuNi, and commercial Pt/C catalysts. The dealloyed AuNi catalyst has a Tafel slope of 53.40 mV dec^{-1} in comparison to 68.78 and 79.47 mV dec^{-1} obtained for as-prepared AuNi and commercial Pt/C catalysts, respectively. It should be noted that the Tafel slopes show typical Temkin adsorption isotherms of oxygenated species, the ORR activity on the dealloyed AuNi catalyst with lower Tafel slope can be effectively enhanced due to the facile oxygen adsorption and the subsequent oxygen reduction.[3, 41]

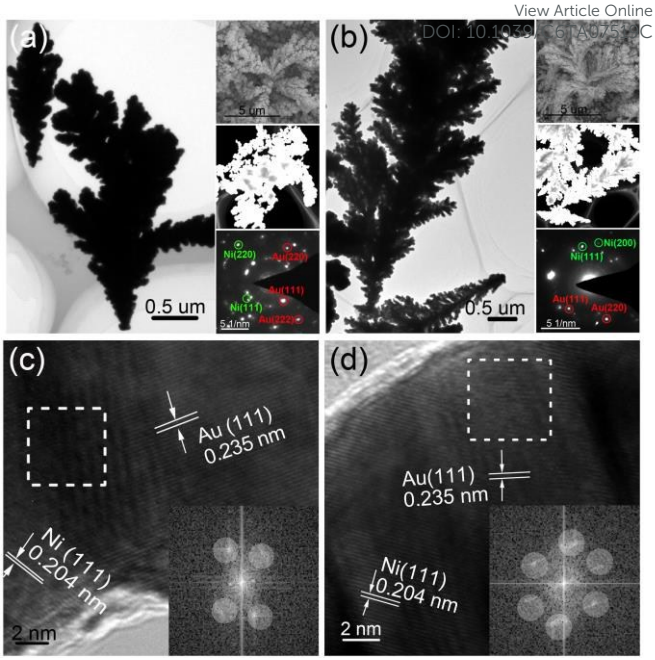

Fig. 2 Bright Field TEM images of (a) as-prepared AuNi and (b) dealloyed AuNi catalysts. The insets for upper, in-between and lower images in both (a) and (b) are the corresponding SEM, dark field TEM and SAED patterns, respectively. HRTEM images of (c) as-prepared AuNi and (d) dealloyed AuNi catalysts. The insets are the corresponding Fast Fourier Transform (FFT) patterns obtained on the area marked by the square.

The above electrochemical measurements indicate that the dealloyed AuNi catalyst shows exceptional ORR activities relative to the commercial Pt/C and even outperforms ever reported Au alloy electrocatalysts in alkaline media (Table S3†). Therefore, the fabricated AuNi catalysts before and after dealloying were further characterized by TEM, SEM, HRTEM, SAED and XPS to investigate the mechanism of the improved catalytic activity. The TEM and SEM images of the as-prepared AuNi catalyst are shown in Fig. 2a, it is clearly observed that the as-prepared AuNi catalyst has the dendritic morphologies with less secondary branches. After

Table 1 The onset potential (E_{onset}, V), half-wave potential ($E_{1/2}$, V), diffusion-limiting current density (j_d, mA cm^{-2}), kinetic current (I_k, mA), electrochemical active surface area (ECSA, cm^2) and the specific activity (SA, mA cm^{-2}) for various catalysts. Standard deviation (SD).

Catalysts name	E_{onset} (V) ±SD	$E_{1/2}$ (V) ±SD	j_d (mA cm^{-2}) ±SD	I_k at 0.8 V (mA) ±SD	ECSA (cm^2) ±SD	SA at 0.8 V (mA cm^{-2}) ±SD
Pure Au	0.90±0.002	0.810±0.001	3.75±0.026	0.52±0.043	3.4±0.013	0.15±0.010
Commercial Pt/C	0.97±0.003	0.829±0.002	4.98±0.014	1.62±0.028	9.0±0.025	0.18±0.005
As-prepared AuNi	1.00±0.002	0.869±0.002	4.86±0.010	3.96±0.022	9.2±0.021	0.43±0.006
Dealloyed AuNi	1.03±0.001	0.896±0.003	4.86±0.017	5.65±0.014	11.5±0.020	0.50±0.008

View Article Online
DOI: 10.1039/C6TA07519C

dealloying, the presence of abundant hierarchical dendrites with side branch tips slitting from the trunk, like "feather", is observed, as shown in Fig. 2b, which leads to higher surface-to-volume ratio. The clear contrast between the skeletons and background shown in the dark field TEM images (in-between insets in Fig. 2a and 2b) further indicates the formation of the developed dendritic structure. According to the previous reports, the hierarchical structures of AuNi dendrites which possess the morphology advantages can profoundly improve the ORR activities.[8, 14, 25] The compositions of the AuNi catalysts were examined by EDX (Table 2), the results show that the Ni contents decrease from 13.75 at % in the as-prepared AuNi catalyst to 5.24 at % in the dealloyed AuNi catalyst, illustrating that the partial Ni atoms are removed by dealloying process, and both the as-prepared and dealloyed samples have Au-enriched surfaces. As seen from Table. S2†, the compositions of these catalysts and the precursor feeding ratios could not quantitatively match quite well. It is rationally attributed to the large potential difference between Au(III) and Ni(II) (Au^{3+}/Au, +1.50 V vs. SHE (standard hydrogen electrode) and Ni^{2+}/Ni, -0.257 V vs. SHE). It can be assumed that Au(III) will be preferentially deposited over the Ni(II) on the GCE, then the preformed Au nanostructures used as nucleic centers facilitate the co-deposition of Ni^{2+} and Au^{3+}. At the surface of the Au, Ni^{2+} cations can be reduced at the less negative potentials due to the underpotential deposition.[42] Actually, we also have performed a control experiment, where almost no nanomaterials were deposited on the GCE surface at -0.6 V vs. SCE in the pure Ni precursor solution, which more firmly verify the above conclusion.

According to the selected area electron diffraction (SAED) patterns (lower insets in the Fig. 2a and 2b), both the as-prepared and dealloyed AuNi catalysts show the typical polycrystalline structures with mixed diffraction rings that belong to face-centered cubic (fcc) structured Au and Ni. The diffraction spots of Au (111), (220), (222) facets and Ni (111), (220) facets are observed for as-prepared AuNi catalyst, and the diffraction spots of Au (111), (220) facets and Ni (111), (200) facets are observed for dealloyed AuNi catalyst. Fig. 2c shows the high-resolution TEM (HRTEM) image of the as-prepared AuNi catalyst, from which the crystalline nature can be analyzed. Based on the HRTEM image, a highly ordered continuous fringe pattern is clearly observed. The crystallographic planes indicate that the spacings of the lattice fringes are 2.35 Å and 2.04 Å, corresponding to (111) plane of face-centered cubic Au and Ni, respectively. As shown in Fig. 2d, the interplanar spacing of 2.35 Å matches with the Au (111) plane and the spacing of 2.04 Å with the Ni (111) for the dealloyed AuNi catalyst.

Table 2 The EDX and XPS composition analysis of as-prepared and dealloyed AuNi catalyst.

Catalysts name	EDX bulk composition (at %)		XPS surface composition (at %)	
	Au	Ni	Au	Ni
As-prepared AuNi	86.25	13.75	86.31	13.69
Dealloyed AuNi	94.76	5.24	95.00	5.00

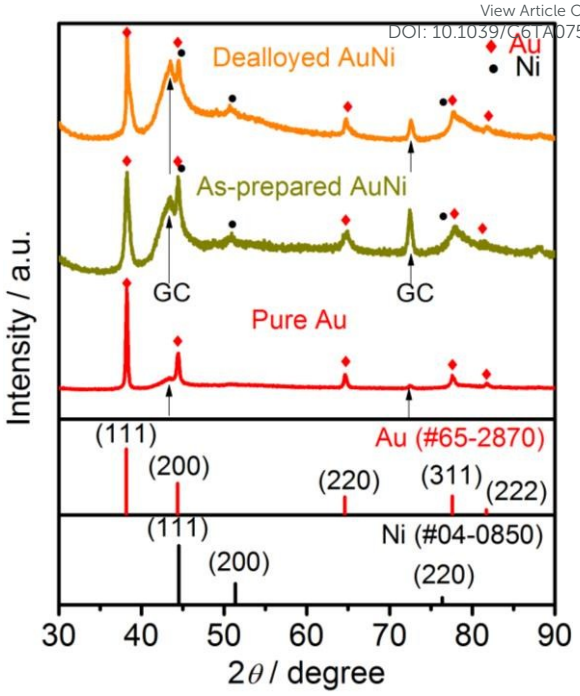

Fig. 3 XRD spectra of the as-prepared AuNi, dealloyed AuNi and pure Au.

The X-ray diffraction (XRD) patterns of pure Au, as-prepared and dealloyed AuNi catalysts are shown in Fig. 3. For as-prepared and dealloyed AuNi catalysts, the typical face-centered cubic phases of metallic Au and Ni are clearly observed. The characteristic diffraction peaks located at 38.24°, 44.4°, 64.6°, 77.6°, and 81.7° are attributed to the (111), (200), (220), (311), and (222) planes of Au for both as-prepared and dealloyed AuNi catalysts. Ni diffraction peaks are observed at 44.5°, 51.8°, and 76.3°, which correspond to (111), (200), and (220) planes, respectively. The broad peak at around 43° is attributed to the glassy carbon. Compared to the corresponding peaks of pure Au, the Au(111) peak positions in the XRD patterns of as-prepared and dealloyed AuNi are slightly shifted (+0.04 degree) and broadened. Based on the Bragg equation, the interplanar spacings of Au (111) in as-prepared and dealloyed AuNi dendrites are 0.2352 nm, which are nearly equal to that of pure Au (0.2354 nm, calculated by Bragg equation). Furthermore, one can note that the intensity of Ni (111) peaks in dealloyed AuNi catalyst visibly decreases, implying the reduction of Ni contents after the dealloying process, which is consistent with the results of EDX and XPS analysis.

X-ray photoelectron spectroscopy (XPS) was further employed to analyze the elemental compositions and surface electron structures of the as-prepared and dealloyed AuNi catalysts. The survey spectra of these two catalysts are shown in Fig. 4a, in which peaks of Au and Ni are clear, and the intensity of Ni decreases greatly after dealloying in comparison to that of as-prepared AuNi catalyst, which is similar with the result of XRD. Specifically, the Ni contents analyzed by XPS in as-prepared and dealloyed AuNi catalysts are 13.69 and 5.0 at %, respectively, which matches well with the EDX results (Table 2), illustrating that the distribution of Ni atoms is uniform in both bulk and surface. Fig. 4b compares the deconvoluted XPS spectra of Ni2p before and after dealloying. The

View Article Online
DOI: 10.1039/C6TA07519C

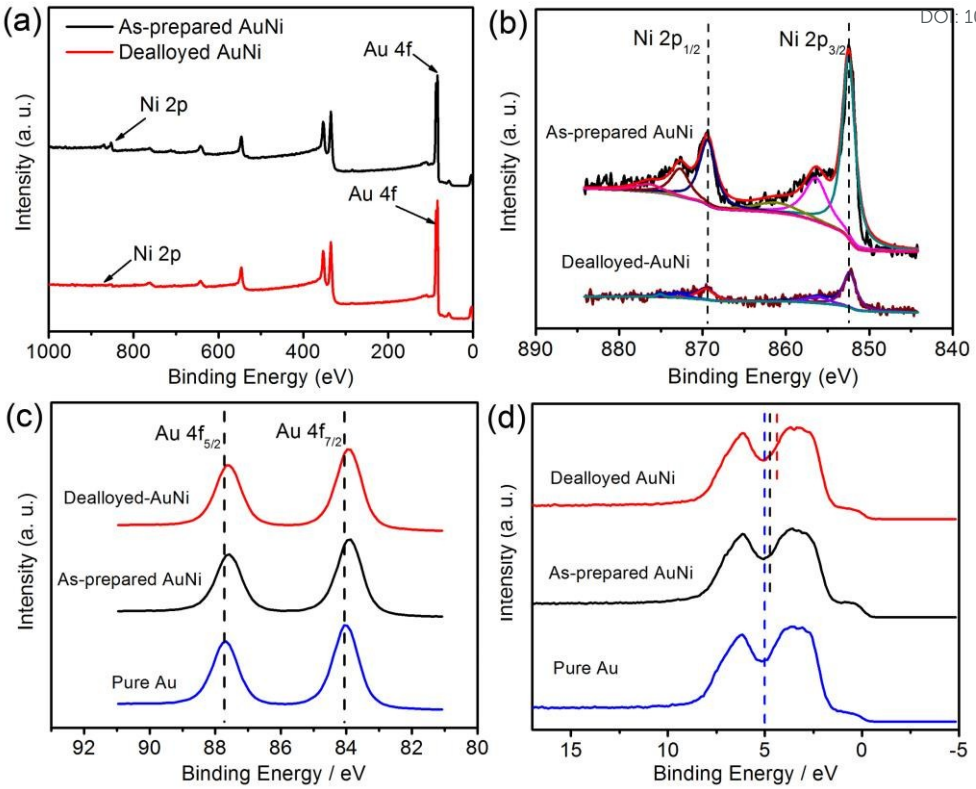

Fig. 4 (a) The XPS survey spectra of the as-prepared AuNi and dealloyed AuNi catalysts. (b) High-resolution Ni2p spectra of the as-prepared AuNi and dealloyed AuNi catalysts. (c) High-resolution Au4f spectra of pure Au, as-prepared AuNi and dealloyed AuNi catalysts. (d) Valence band spectrum (VBS) of the pure Au, as-prepared AuNi and dealloyed AuNi catalysts.

binding energies of $Ni2p_{1/2}$ and $Ni2p_{3/2}$ orbits are 869.5 and 852.3 eV for both samples, which are the same as the binding energies of Ni^0 atom,[43] indicating the formation of metallic Ni. Moreover, the characteristic satellite peaks are observed at 872.7 and 856.3 eV of $Ni2p_{1/2}$ and $Ni2p_{3/2}$. These satellite peaks can be attributed to $Ni(OH)_2$, which is in good agreement with the previous literature.[44, 45] Fig. 4c depicts the Au4f core-level (CL) of pure Au, as-prepared and dealloyed AuNi catalysts. Pure Au displays a doublet with the binding energies located at 87.7 and 84.1 eV for $Au4f_{5/2}$ and $Au4f_{7/2}$, respectively, corresponding to the zero-valence Au.[14, 31] Compared to pure Au catalyst, the binding energies for both as-prepared AuNi (87.6 and 83.9 eV) and dealloyed AuNi (87.5 and 83.9 eV) shift to the lower values.[43, 46] Previous reports show that the shift in binding energies is associated with the variation in the d-band center. A CL shift to a lower binding energy value means that a positive shift in d-band center with respect to the Fermi level,[21] which favors Au with stronger oxygen absorption energy and higher ORR activity. To further determine this conclusion, the valence band spectrum (VBS) of these three catalysts were also measured, as shown in Fig. 4d, the d-band center of dealloyed AuNi (red dashed line) is closer to the Fermi energy level than those of as-prepared AuNi (black dashed line) and pure Au (blue dashed line). Therefore, it can be concluded that the electronic effect explained by the d-bond theory play a major role in improving the ORR activity of the AuNi catalyst.[18, 19, 47]

To further examine the reaction pathway and kinetics of AuNi catalysts towards oxygen reduction reaction, the linear sweep voltammetry (LSV) curves were taken on a rotating disk electrode from 400 to 2000 rpm. One can see from Fig. 5a, c and Fig. S6a, c† that the catalytic current densities increase with an increase in the rotating rates, which indicates that the catalytic reaction of the AuNi catalysts for ORR is controlled by the mass transport of O_2 to the surface of the catalysts.[4] The electron-transfer number was further analyzed by the Koutecky-Levich (K-L) plots, as the disk voltammetric current density (j) may involve both kinetic (j_k) and diffusion-limiting (j_d) current densities contributions. The K-L plots show the inverse current density (j^{-1}) as a function of the inverse of the square root of the rotating speed ($\omega^{-1/2}$). The slopes of their linear fit lines are used to calculate the electron transfer number (n). The Koutecky-Levich equation is expressed in Eq 1-3:[48]

$$j^{-1} = j_k^{-1} + j_d^{-1} = j_k^{-1} + (B\omega^{1/2})^{-1} \quad (1)$$

$$B = 0.62nFC_0D_0^{2/3}v^{-1/6} \quad (2)$$

$$j_k = nFkC_0 \quad (3)$$

Where j is the measured current density, j_k and j_d are the kinetic and diffusion-limiting current densities of the ORR, respectively, B is the Levich slope, ω is the angular velocity of the disk ($\omega = 2\pi f$, f is the linear rotation speed in rpm), n is the overall number of the electrons transferred during O_2 reduction, F is the Faraday constant (96485 C mol^{-1}), C_0 denotes the bulk concentration of O_2 (1.2×10^{-6}

View Article Online
DOI: 10.1039/C6TA07519C

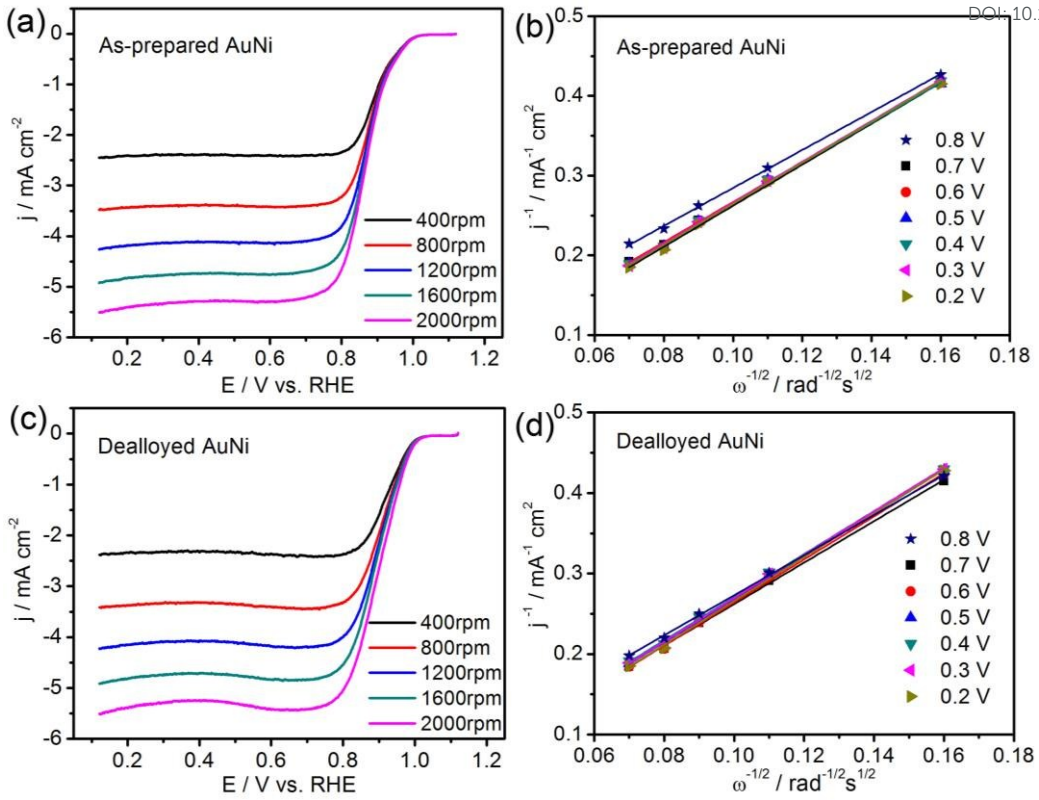

Fig. 5 The rotation-rate-dependent ORR polarization curves of (a) as-prepared AuNi and (c) dealloyed AuNi catalysts in O_2-saturated 0.1 M KOH solution with a sweep rate of 10 mV s^{-1}. The Koutecky-Levich plots (j^{-1} vs. $\omega^{-1/2}$) of (b) as-prepared AuNi and (d) dealloyed AuNi catalysts at different potentials.

mol cm^{-3}), D_0 represents the diffusion coefficient of O_2 (1.9×10^{-5} cm^2 s^{-1}) in 0.1 M KOH aqueous solution, v is the kinetic viscosity of the electrolyte (0.01 cm^2 s^{-1}).[49, 50]

Fig. 5b, d and Fig. S6b, d† show the corresponding K-L plots of the as-prepared AuNi, dealloyed AuNi, Pt/C and pure Au catalysts over the potential range of 0.2 to 0.8 V. It can be seen from the K-L plots that all the experimental data show good linearity within the corresponding potential range, indicating a first-order reaction with respect to dissolved oxygen.[3, 12] The number of electrons transferred per oxygen molecule for as-prepared AuNi, dealloyed AuNi, commercial Pt/C and pure Au catalysts are derived to be 3.8, 3.9, 4.0 and 2.8 at 0.7 V, respectively. The calculated results exhibit that the ORR catalyzed by dealloyed AuNi and as-prepared AuNi catalysts occur through a four-electron pathway, *i.e.*, direct reduction of O_2 to OH^-, which is similar to that by commercial Pt/C catalyst[51] and superior to that by pure Au. Furthermore, the transferred electron numbers (n) at other potentials of these catalysts are listed in Fig. S7†, the numbers of electrons transferred during ORR for all the catalysts are almost constant with the variety of potentials. Besides, the rotation-rate-dependent ORR polarization curves and the corresponding K-L plots of other catalysts involved in our experiments are also shown in Fig. S8†.

The catalytic stability of the catalyst in an electrochemical environment is important for their realistic applications.[3, 52] Here, the catalytic durability of dealloyed AuNi and commercial Pt/C catalysts were evaluated by applying continuous potential cycling (5,000 cycles) between 0.5 and 1.0 V with a scan rate of 100 mV s^{-1} in O_2-saturated 0.1 M KOH solution at room temperature. ECSAs and LSV polarization curves at 1600 rpm for these two catalysts before and after the potential cycling have been measured to investigate the degradation of catalytic activities. As shown in Fig. 6, it is obvious that the dealloyed AuNi catalyst exhibits excellent long-

Table 3 Comparison of the electrochemical activity of dealloyed AuNi with commercial Pt/C before and after potential cycling.

Catalysts name	Before cycling				After cycling				Variation		
	E_{onset} (V)	$E_{1/2}$ (V)	j_d (mA cm^{-2})	SA (mA cm^{-2})	E_{onset} (V)	$E_{1/2}$ (V)	j_d (mA cm^{-2})	SA (mA cm^{-2})	Δ $E_{1/2}$ (mV)	Δ j_d (%)	Δ ECSA (%)
Commercial Pt/C	0.97	0.829	4.98	0.18	0.93	0.769	4.17	0.07	60	19	44.7
Dealloyed AuNi	1.03	0.896	4.86	0.50	1.01	0.858	4.66	0.36	38	4.3	27.6

View Article Online
DOI: 10.1039/C6TA07519C

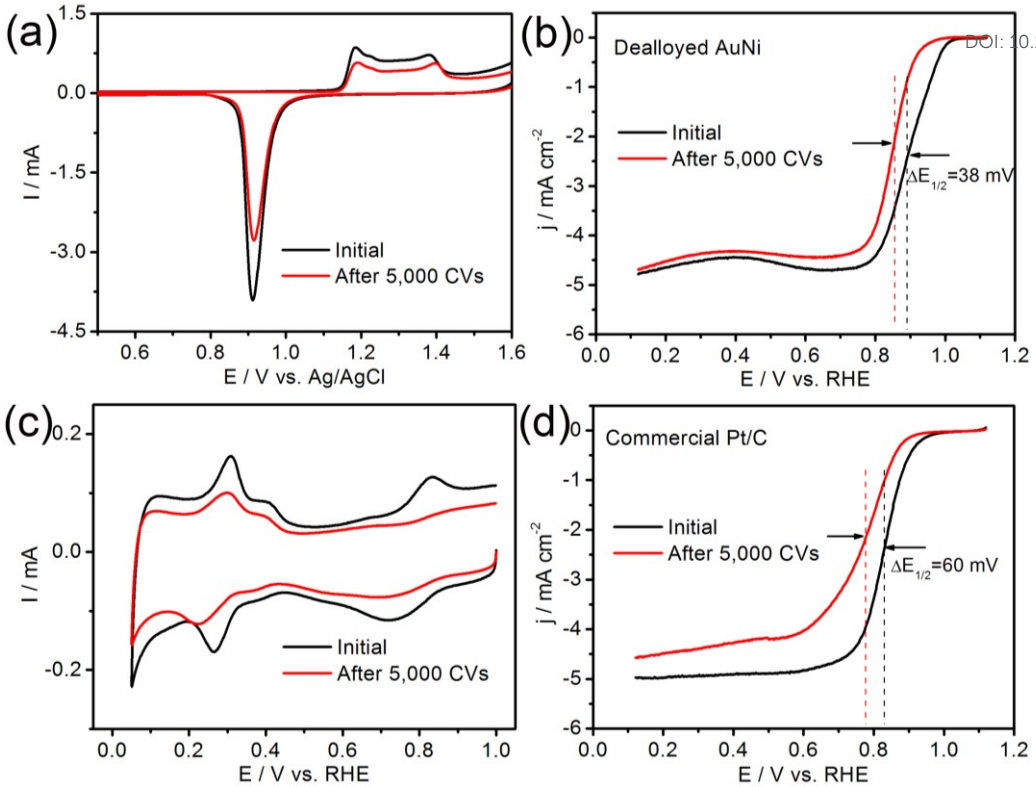

Fig. 6 Comparison of ORR activities of dealloyed AuNi dendrites and commercial Pt/C before and after 5,000 cycles. (a) CV curves of dealloyed AuNi dendrites in N_2-saturated 0.5 M H_2SO_4 solution at a sweep rate of 50 mV s^{-1}. (b) ORR polarization curves of dealloyed AuNi dendrites in O_2-saturated 0.1 M KOH solution. (c) CV curves of Pt/C in N_2-saturated 0.1 M KOH solution with a sweep rate of 50 mV s^{-1}. (d) ORR polarization curves of Pt/C in O_2-saturated 0.1 M KOH solution.

term stability compared with commercial Pt/C catalyst under the same test condition. Over continuous potential cycling, the dealloyed AuNi catalyst shows only 38 mV negative shift in the half-wave potential and a loss of 4.3 % relative to the initial diffusion-limiting current density, and its ECSA remains a high value of 72.4% of the pristine surface area. In contrast, commercial Pt/C catalyst exhibits a more negative shift of 60 mV (Table 3) in $E_{1/2}$ and loses 19 % of the diffusion-limiting current density, and undergoes a nearly 44.7% loss in ECSA after 5,000 cycles. It is widely accepted that Pt nanoparticles usually suffer Ostwald ripening and tend to form larger particles, leading to the significant decrease in the ECSA and the catalytic activity. Moreover, the carbon corrosion also accelerates its more severe loss of ORR activity.[53] However, the dealloyed AuNi catalyst in our experiment was synthesized without the carbon support, thus, avoiding the carbon corrosion problem. More importantly, the enhanced stability of the dealloyed AuNi catalyst is probably attributed to the stability of dendrite structure caused by the Au-rich surfaces after electrochemical deposition and dealloying.[21, 54] The structure and morphology evolution of the dealloyed AuNi dendrites before and after the potential cycling were observed by TEM. Fig. S9† shows that there is not obvious change in the structure and morphology of this dealloyed AuNi dendrites. Therefore, these experimental observations suggest the dealloyed AuNi catalyst be a promising alternative for Pt forms as effective cathode catalyst for ORR in basic solution.

Conclusion

In summary, this work presents a facile method to synthesize the high-performance AuNi catalyst for oxygen reduction reaction in alkaline media. The synthesized AuNi catalyst is tailored to be the dendritic morphology by electrodepositon and dealloying approach. The dealloyed AuNi catalyst exhibits significantly enhanced catalytic activity and durability after 5,000 potential cycling in comparison with the state-of-the-art Pt/C catalyst. The improvement of the ORR catalytic activity for dealloyed AuNi can be ascribed to the unique morphology and electronic effect characterized by TEM and XPS. Consequently, the dealloyed AuNi dendrite is a potential candidate as the advanced ORR catalyst with excellent electrochemical activity, high cycling stability, and easy preparation in the field of the renewable energy technologies.

Acknowledgements

This study was supported by the National Natural Science Foundation of China (grant nos. 51271148 and 50971100), the Research Fund of State Key Laboratory of Solidification Processing in China (grant no. 150-ZH-2016), the Aeronautic Science Foundation Program of China (grant no. 2012ZF53073), the Science and Technology Innovation Fund of Western Metal Materials (grant no. XBCL-2-11) and the Doctoral Fund of Ministry of Education of China (grant no. 20136102110013).

References

1 Y. Li and H. Dai, *Chem. Soc. Rev.*, 2014, **43**, 5257.
2 Y. Li, M. Gong, Y. Liang, J. Feng, J.-E. Kim, H. Wang, G. Hong, B. Zhang and H. Dai, *Nat. Commun.*, 2013, **4**, 1805.
3 V. M. Dhavale and S. Kurungot, *ACS Catal.*, 2015, **5**, 1445.
4 Y. Jin and F. Chen, *Electrochim. Acta*, 2015, **158**, 437.
5 Z. Chen, A. Yu, D. Higgins, H. Li, H. Wang and Z. Chen, *Nano Lett.*, 2012, **12**, 1946.
6 C. Xu, Y. Liu, Q. Hao and H. Duan, *J. Mater. Chem. A*, 2013, **1**, 13542.
7 X. Ge, A. Sumboja, D. Wuu, T. An, B. Li, F. T. Goh, T. A. Hor, Y. Zong and Z. Liu, *ACS Catal.*, 2015, **5**, 4643.
8 D. S. He, D. He, J. Wang, Y. Lin, P. Yin, X. Hong, Y. Wu and Y. Li, *J. Am. Chem. Soc.*, 2016, **138**, 1494.
9 A. Holewinski, J.-C. Idrobo and S. Linic, *Nat. Chem.*, 2014, **6**, 828.
10 D. A. Slanac, W. G. Hardin, K. P. Johnston and K. J. Stevenson, *J. Am. Chem. Soc.*, 2012, **134**, 9812.
11 J. Wu, S. Shan, J. Luo, P. Joseph, V. Petkov and C.-J. Zhong, *ACS Appl. Mater. Interfaces*, 2015, **7**, 25906.
12 Y. Song, K. Liu and S. Chen, *Langmuir*, 2012, **28**, 17143.
13 H. Yin, H. Tang, D. Wang, Y. Gao and Z. Tang, *ACS Nano*, 2012, **6**, 8288.
14 X.-R. Li, X.-L. Li, M.-C. Xu, J.-J. Xu and H.-Y. Chen, *J. Mater. Chem. A*, 2014, **2**, 1697.
15 S. Xu and P. Wu, *J. Mater. Chem. A*, 2014, **2**, 13682.
16 M. Govindhan and A. Chen, *J. Power Sources*, 2015, **274**, 928.
17 S. S. Kim, Y. R. Kim, T. D. Chung and B. H. Sohn, *Adv. Funct. Mater.*, 2014, **24**, 2764.
18 J. K. Nørskov, J. Rossmeisl, A. Logadottir, L. Lindqvist, J. R. Kitchin, T. Bligaard and H. Jonsson, *J. Phys. Chem. B*, 2004, **108**, 17886.
19 F. Lima, J. Zhang, M. Shao, K. Sasaki, M. Vukmirovic, E. Ticianelli and R. Adzic, *J. Phys. Chem. C*, 2007, **111**, 404.
20 D. Wang, H. L. Xin, R. Hovden, H. Wang, Y. Yu, D. A. Muller, F. J. DiSalvo and H. D. Abruña, *Nat. Mater.*, 2013, **12**, 81.
21 X. Tan, S. Prabhudev, A. Kohandehghan, D. Karpuzov, G. A. Botton and D. Mitlin, *ACS Catal.*, 2015, **5**, 1513.
22 X. Wu, F. Chen, Y. Jin, N. Zhang and R. L. Johnston, *ACS Appl. Mater. Interfaces*, 2015, **7**, 17782.
23 K. Shin, D. H. Kim and H. M. Lee, *ChemSusChem*, 2013, **6**, 1044.
24 K. Shin, D. H. Kim, S. C. Yeo and H. M. Lee, *Catal. Today*, 2012, **185**, 94.
25 X. Huang, Z. Zhao, L. Cao, Y. Chen, E. Zhu, Z. Lin, M. Li, A. Yan, A. Zettl and Y. M. Wang, *Science*, 2015, **348**, 1230.
26 Y. Xu, S. Hou, Y. Liu, Y. Zhang, H. Wang and B. Zhang, *Chem. Commun.*, 2012, **48**, 2665.
27 X. Huang, E. Zhu, Y. Chen, Y. Li, C. Y. Chiu, Y. Xu, Z. Lin, X. Duan and Y. Huang, *Adv. Mater.*, 2013, **25**, 2974.
28 M. Wang, W. Zhang, J. Wang, D. Wexler, S. D. Poynton, R. C. Slade, H. Liu, B. Winther-Jensen, R. Kerr and D. Shi, *ACS Appl. Mater. Interfaces*, 2013, **5**, 12708.
29 L. Chen, H. Guo, T. Fujita, A. Hirata, W. Zhang, A. Inoue and M. Chen, *Adv. Funct. Mater.*, 2011, **21**, 4364.
30 M. H. Tang, C. Hahn, A. J. Klobuchar, J. W. D. Ng, J. Wellendorff, T. Bligaard and T. F. Jaramillo, *Phys. Chem. Chem. Phys.*, 2014, **16**, 19250.
31 T. Yang, C. M. R. de Almeida, D. Ramasamy and F. J. A. Loureiro, *J. Power Sources*, 2014, **269**, 46.
32 M. G. Hosseini, M. Abdolmaleki and F. Nasirpouri, *Electrochim. Acta*, 2013, **114**, 215.
33 F. Xiao, L. Yang, F. Zhao and B. Zeng, *Anal. Bioanal. Electrochem.*, 2013, **5**, 154.
34 H.-B. Noh, M. H. Naveen, Y.-J. Choi, E. S. Choe and Y.-B. Shim, *Chem. Commun.*, 2015, **51**, 6659.
35 M. H. Naveen, N. G. Gurudatt, H. B. Noh and Y. B. Shim, *Adv. Funct. Mater.*, 2016, **26**, 1590.
36 N. Tian, Z.-Y. Zhou, S.-G. Sun, Y. Ding and Z. L. Wang, *science*, 2007, **316**, 732.
37 B. Lim, M. Jiang, P. H. Camargo, E. C. Cho, J. Tao, X. Lu, Y. Zhu and Y. Xia, *science*, 2009, **324**, 1302.
38 X. Chen, C. H. Cui, Z. Guo, J. H. Liu, X. J. Huang and S. H. Yu, *Small*, 2011, **7**, 858.
39 S. Trasatti and O. Petrii, *Pure Appl. Chem.*, 1991, **63**, 711.
40 Z. Zhang, Z. Luo, B. Chen, C. Wei, J. Zhao, J. Chen, X. Zhang, Z. Lai, Z. Fan and C. Tan, *Adv. Mater.*, 2016, **28**, 8712.
41 S. Knani, L. Chirchi, W. Napporn, S. Baranton, J. Léger and A. Ghorbel, *J. Electroanal. Chem.*, 2015, **738**, 145.
42 K.-H. Choi, Y. Jang, D. Y. Chung, P. Seo, S. W. Jun, J. E. Lee, M. H. Oh, M. Shokouhimehr, N. Jung and S. J. Yoo, *Chem. Commun.*, 2016, **52**, 597.
43 J. Rousset, F. Cadete Santos Aires, B. Sekhar, P. Mélinon, B. Prevel and M. Pellarin, *J. Phys. Chem. B*, 2000, **104**, 5430.
44 J. W. Lee, T. Ahn, D. Soundararajan, J. M. Ko and J.-D. Kim, *Chem. Commun.*, 2011, **47**, 6305.
45 J. Yan, W. Sun, T. Wei, Q. Zhang, Z. Fan and F. Wei, *J. Mater. Chem.*, 2012, **22**, 11494.
46 H. Chen, J. Huang, D. Huang, D. Sun, M. Shao and Q. Li, *J. Mater. Chem. A*, 2015, **3**, 4846.
47 Y. Jiao, Y. Zheng, M. Jaroniec and S. Z. Qiao, *Chem. Soc. Rev.*, 2015, **44**, 2060.
48 A. J. Bard and L. R. Faulkner, *Electrochemical Methods, 2nd ed.; Wiley: New York*, 2001.
49 Y. Jin, F. Chen, Y. Lei and X. Wu, *ChemCatChem*, 2015, **7**, 2377.
50 W. Chen and S. Chen, *Angew. Chem. Int. Ed.*, 2009, **48**, 4386.
51 J. H. Shim, Y. S. Kim, M. Kang, C. Lee and Y. Lee, *Phys. Chem. Chem. Phys.*, 2012, **14**, 3974.
52 I. Takahashi and S. S. Kocha, *J. Power Sources*, 2010, **195**, 6312.
53 Z. Chen, M. Waje, W. Li and Y. Yan, *Angew. Chem. Int. Ed.*, 2007, **46**, 4060.
54 X. Sun, D. Li, Y. Ding, W. Zhu, S. Guo, Z. L. Wang and S. Sun, *J. Am. Chem. Soc.*, 2014, **136**, 5745.

View Article Online
DOI: 10.1039/C6TA07519C

AuNi hierarchical dendrites were fabricated by facile electrodeposition and dealloying method with exceptional ORR activity and remarkable long-term stability.